DOI: 10.1002/chem.200701638

Electroactive Nanorods and Nanorings Designed by Supramolecular Association of π-Conjugated Oligomers

Olivier J. Dautel,*[a] Mike Robitzer,[a] Jean-Charles Flores,[a] Denis Tondelier,[b] Françoise Serein-Spirau,[a] Jean-Pierre Lère-Porte,*[a] David Guérin,[b] Stéphane Lenfant,[b] Monique Tillard,[c] Dominique Vuillaume,*[b] and Joël J. E. Moreau[a]

Abstract: In investigations into the design and isolation of semiconducting nano-objects, the synthesis of a new bisureido π-conjugated organogelator has been achieved. This oligo(phenylenethienylene) derivative was found to be capable of forming one-dimensional supramolecular assemblies, leading to the gelation of several solvents. Its self-assembling properties have been studied with different techniques (AFM, EFM, etc.). Nano-objects have successfully been fabricated from the pristine organogel under appropriate dilution conditions. In particular, nanorods and nanorings composed of the electroactive organogelator have been isolated and characterized. With additional support from an electrochemical study of the organogelator in solution, it has been demonstrated by the EFM technique that such nano-objects were capable of exhibiting charge transport properties, a requirement in the fabrication of nanoscale optoelectronic devices. It was observed that positive charges can be injected and delocalized all along an individual nano-object (nanorod and nanoring) over micrometers and, remarkably, that no charge was stored in the center of the nanoring. It was also observed that topographic constructions in the nanostructures prevent transport and delocalization. The same experiments were performed with a negative bias (i.e., electron injection), but no charge delocalization was observed. These results could be correlated with the nature of **1**, which is a good electron-donor, so it can easily be oxidized, but can be reduced only with difficulty.

Keywords: nanorings · nanorods · pi-conjugated oligomers · self-assembly · supramolecular chemistry

Introduction

One of the most promising "bottom-up" approaches in nanoelectronics is to assemble π-conjugated molecules to build nano-sized electronic and opto-electronic devices in the 5–100 nm length scale. This field of research, called "supramolecular electronics" by Meijer's group, bridges the gap between molecular electronics and bulk "plastic" electronics.[1] In this context, the design and preparation of nanowires are of considerable interest for the development of nano-electronic devices such as nanosized transistors,[2] sensors,[3] logic gates,[4] light-emitting diodes,[5] and photovoltaic devices.[6]

Of all the noncovalent interactions, hydrogen bonds have been most extensively used to construct supramolecular architectures, as they are highly selective and directional not only in solution but also on surfaces. Numerous nanostructures such as nanorods, nanotubes, or nanorings have been obtained by this approach. In particular, the use of organogelators as directors to control the morphologies of the aggregates has been explored recently. Cholesterol- and phospholipid-tethered *trans*-stilbenes are able to gelate different

[a] Dr. O. J. Dautel, Dr. M. Robitzer, Dr. J.-C. Flores, Prof. F. Serein-Spirau, Prof. J.-P. Lère-Porte, Prof. J. J. E. Moreau
Architectures Moléculaires et Matériaux Nanostructurés
Institut Charles Gerhardt Montpellier, UMR CNRS 5253
Ecole Nationale Supérieure de Chimie de Montpellier
8 rue de l'Ecole Normale
34296 Montpellier Cedex 05 (France)
Fax: (+33) 467-147-212
E-mail: olivier.dautel@enscm.fr
jean-pierre.lere-porte@enscm.fr

[b] Dr. D. Tondelier, Dr. D. Guérin, Dr. S. Lenfant, Dr. D. Vuillaume
Molecular Nanostructures and Devices group
Institut d'Electronique, de Micro-électronique et de Nanotechnologie
CNRS UMR 8520, BP0069, Avenue Poincare
59652 Villeneuve d'Ascq, cedex (France)
Fax: (+33) 320-197-884
E-mail: dominique.vuillaume@iemn.univ-lille1.fr

[c] Dr. M. Tillard
Agrégats, Interfaces, Matériaux pour l'Énergie
Institut Charles Gerhardt, UMR 5253 CNRS UM2, CC015
Université de Montpellier 2, Sciences et Techniques du Languedoc
2 Place Eugène Bataillon
34095 Montpellier Cedex 5 (France)

Supporting information for this article is available on the WWW under http://www.chemeurj.org/ or from the author.

organic solvents in which the steroid and lipid units serve as templates to form one-dimensional stacks.[7] However, organogelators based on π-conjugated systems, unlike systems based on dyes, are relatively rare. Ajayaghosh et al. extended this concept to oligophenylenevinylene (OPV) derivatives and reported a completely thermoreversible self-assembly process in a series of hydrocarbon solvents from single OPV molecules to fibers and ultimately to an entangled network structure.[8] The absorption and emission properties showed dramatic changes during gelation, which is an indication of strong intermolecular π electronic coupling of the ordered OPV segments. In a similar way, van Esch et al. have shown by the pulse-radiolysis time-resolved microwave conductivity (PR-TRMC) technique on solid-state powder samples that high charge carrier mobilities can be achieved in gel networks based on thiophene and bithiophene derivatives modified with bisurea units. The thiophene moieties formed closely packed arrays enforced by the urea hydrogen-bonding units, thereby creating an efficient pathway for charge transport.[9,10] The two-dimensional self-assembly of the bisurea 1,2-thiophene has been studied on solid substrates. Elongated twisted fibers with lengths of 20–100 μm and widths of 2–10 μm were observed on SiO_2. These fibers are strongly birefringent, indicating a high degree of molecular ordering. After annelation, extended mono-layers consisting of upright 1D arrays standing side-by-side are formed. On highly orientated pyrolytic graphite, 1D arrays lying flat on the surface were obtained. Scanning tunneling spectroscopy indicated that effective conjugation in the π stacks exists, as the band gap of the thiophene was decreased.[11] As pointed out by Shenning and Meijer, it would be of great interest if we were able to study such types of fibers made up of molecules containing longer conjugated π fragments.[12]

Furthermore, progress needs to be achieved in order to demonstrate that individual nano-objects might be capable of exhibiting electronic properties such as charge transport, a requirement in the fabrication of nanoscale optoelectronic devices.

In this context, here we report the synthesis of **1**, a sequence of five 1,4-dialkoxyphenylene and thiophene units functionalized with two urea moieties. The π-conjugated core is defined by the regular alternation of thienylene and 1,4-dialkoxyphenylene. We have demonstrated by PES/UV spectroscopy correlated with DFT calculations that thiophene and dialkoxyphenylene fragments are suitable for the construction of fully π-conjugated oligomers. Because of noncovalent S···O interactions the fragments are coplanar, while in addition, the energy levels of the π-molecular orbitals are close.[13] As a result, a strong interaction between the molecular orbitals of the thiophene and the dialkoxyphenylene fragments destabilizes the HOMO levels of the oligomer. This type of compound therefore exhibits a low oxidation potential and a relatively low HOMO–LUMO gap. This fully π-conjugated core was disubstituted with two urea moieties in order to take advantage of their self-assembly properties, resulting from the strong directional abilities of hydrogen bonds. With regard to previous work,[14] a propylene arm spacer was adopted to favor the self-association of neutral or oxidized π segments.

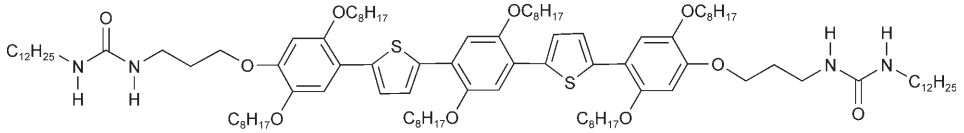

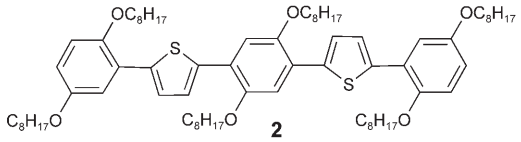

In order to increase the solubility of the compound and to improve the supramolecular organization through van der Waals interactions, two alkoxy chains were also grafted onto each benzene ring. This oligo(phenylenethienylene) derivative was found to be capable of forming one-dimensional supramolecular assemblies, leading to gelation of several solvents. Its self-assembling properties have been studied by different techniques.

To confirm the influence of the urea moieties on the supramolecular organization of **1** in the solid state, the otherwise identical unsubstituted conjugated segment **2** was prepared, and the structural and optical properties of the two compounds were established and compared. Nano-objects were successfully fabricated from the pristine organogel of **1** under appropriate dilution conditions. In particular, nanorods and nanorings composed of the electroactive organogelator were isolated and characterized. With additional support from an electrochemical study of the solution, it was possible to demonstrate by the EFM technique that such nano-objects were capable of exhibiting charge transport properties. Unlike PR-TMC experiments, this technique can provide direct evidence of charge delocalization on an individual nano-object. Because of the ultrahigh frequencies (GHz) and low field strengths (about $10\,V\,cm^{-1}$) used, the mobility values obtained by PR-TMC experiments mainly reflect the mobilities of charge carriers within the best organized domains (i.e., highest mobility) within a material.[15] The use of nanosecond time resolution ensures in addition that in most cases the charge carriers are probed prior to their diffusional drift to intrinsic chemical or physical trapping sites. On the other hand, EFM images of an individual object will reflect how far charge carriers move within the object and the influence of defects (grain and domain boundaries) on their mobility.

Results and Discussion

Synthesis of the organogelator: Compound **1** was synthesized in ten steps from 1,4-dioctyloxybenzene (**3**) and 2,5-dioctyloxy-1,4-phenylenediboronic acid as shown in Scheme 1.[16] In a Friedel–Crafts acylation reaction, compound **3** was converted into the corresponding ketone **4** in 85% yield. In two steps, **4** was then transformed into phenol **5** in 80% yield by a Baeyer–Villiger reaction followed by a saponification.[17,18] *O*-Alkylation of **5** with *N*-(3-bromopropyl)phthalimide (72%) and iodination with *N*-iodosuccinimide (NIS) in the presence of 0.3 equiv of trifluoroacetic acid as a catalyst[19] gave **7** in 95% yield. Suzuki cross-coupling of **7** with thiophene-2-boronic acid afforded **8** in 71% yield. Iodination with NIS gave an 89% yield of **9**, which on Suzuki cross-coupling with 2,5-dioctyloxy-1,4-phenylenediboronic acid afforded **10** in 53% yield. The last two steps consisted of cleaving the two phthalimides by hydrazinolysis to recover the diamine (96%), which reacted with 2.2 mol equivalents of dodecyl isocyanate to afford the bisurea **1** in 95% yield. This multi-step synthesis of compound **1** constitutes a versatile and general procedure by which to functionalize π-conjugated oligomers with urea moieties.

Study of the organogel: Compound **1** is soluble in common solvents (THF, toluene, dichloromethane, etc.). When solutions of **1** (10 mg) in toluene or dichloromethane (1 mL) were heated, however, organogels were formed upon cooling the solution to −20 °C. After their formation, the different organogels were stable at room temperature. In the same way, **1** gelatinized toluene, THF, and even the nonpolar and hydrophobic tetrachloroethylene at concentrations as low as 0.2 wt%. Tetrachloroethylene was the solvent chosen for the organogel studies for two major reasons: i) it does not absorb infra-red radiation, which is essential in order to permit study of the contribution of the hydrogen bond interaction by FTIR, and ii) its high boiling point (105 °C) should allow examination of the energy required to break the hydrogen bond system of the urea function.

The organogel was prepared as follows: compound **1** (5 mg mL^{-1}, 0.3 wt%) was dissolved in hot tetrachloroethylene and the mixture was allowed to stand at −20 °C, giving an opaque, yellow organogel. By the "tilting" method, the sol–gel phase transition temperature (T_{gel}) was found to be around 50 °C.[20] The sol–gel transition was studied as a function of the gel concentration.

Two methods were used to determine the gelation temperature: the ball-drop method[21] and test tube "tilting" (see Supporting Information). In the first method, a steel ball with a definite weight is placed on the gel. The samples tubes are placed in a water bath and the temperature is increased slowly. T_{gel} is taken as the temperature at which the ball touches the bottom of the tube. In the second method, the gelation temperature was determined by tilting the test tube containing the solution. The sample vials were immersed in tilted positions in a water bath and the temperature was increased slowly. T_{gel} is taken as the temperature at which the gel started to flow. In both methods, the T_{gel} values increased linearly with concentration over the 0.1–0.6 wt% range and then became independent of concentration up to at least 1 wt%: under these last conditions the $T_{gel\,max}$ was (66±1) °C in both cases. This behavior is commonly observed for organogels.[22] However, for concentrations lower than 0.5 wt%, a slight shift toward lower temperatures was observed in the T_{gel} determined by the ball-drop method, due to the heavy ball (450 mg per ball) going through the network even if the fibers were still present. The hydrogen bond pattern of the urea can be studied by Fourier Transform Infra-Red (FTIR) spectroscopy.[23] Indeed, it can be described in terms of two symmetrical hydrogen bonds between the carbonyl function of one urea moiety and the secondary amines of another vicinal urea molecule.

A urea function is characterized by three infra-red absorption bands corresponding to the N–H stretch (asym ν_{NH} =

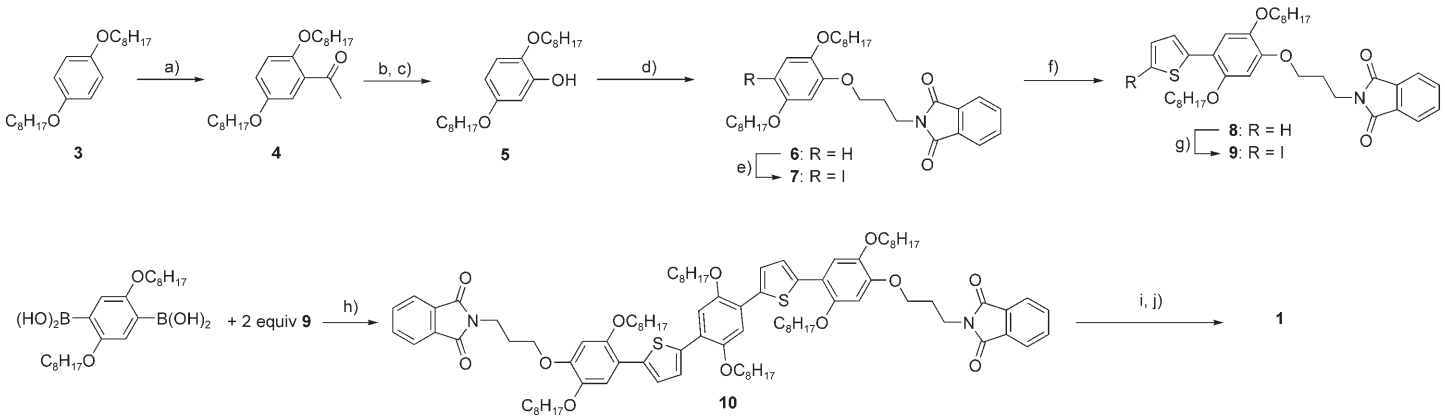

Scheme 1. Synthesis of **1**. a) 2 equiv acetyl chloride, 1.2 equiv $AlCl_3$, CH_2Cl_2, 40 °C, 16 h, 85%; b) peracetic acid, AcOEt, 40 °C, 16 h; c) 4 equiv KOH, 2 equiv EtOH, H_2O, 80 °C, 1 h 30, then 4 equiv HCl (1.5 N), −30 °C, 80%; d) K_2CO_3, *N*-(3-bromopropyl)phthalimide, acetonitrile, 21 °C, 72%; e) NIS, 0.3 equiv CF_3COOH, CH_2Cl_2, 21 °C, 95%; f) thiophene-2-boronic acid, [Pd_2dba_3], PPh_3, Na_2CO_3, THF/H_2O, 70 °C, 71%; g) NIS, CH_2Cl_2, 21 °C, 89%; h) Pd_2dba_3, PPh_3, Na_2CO_3, THF/H_2O, 70 °C, 53%; i) $NH_2NH_2{\cdot}H_2O$, THF, 66 °C, 96%; j) 2.2 equiv dodecylisocyanate, CH_2Cl_2, 40 °C, 95%. Overall yield 15%.

3357 and sym $\nu_{NH} = 3325\ cm^{-1}$), the C=O stretch called the "amide I band" ($\nu_{CO} \approx 1627\ cm^{-1}$), and a combination of the N–H deformation and of the C–N stretch called the "amide II band" ($\delta_{NH}+\nu_{CN} \approx 1576\ cm^{-1}$). The intensities and the wavenumbers of those three bands are directly related to the hydrogen bond strength of the system. In the case of a transition from an associated urea to a free urea, the N–H stretch and amide I bands are shifted to higher wavenumbers and the amide II band to lower wavenumbers. In this context, a tetrachloroethylene gel of **1** (5 mg mL^{-1}, 0.3 wt %) was introduced into a sealed KBr cell and the FTIR spectra were recorded at different temperatures (Figure 1).

At room temperature, the amide I and the amide II bands, found at 1627 and 1576 cm^{-1}, respectively, are representative of an associated urea function. With increasing temperature, the intensities of the two bands are lowered and two new bands appear at 1694 and 1515 cm^{-1}. The occurrence of an isobestic point at 1657 cm^{-1} demonstrated the presence of one-mode association alternation of urea functions and of equilibrium between the free and the associated species. At ≈60–65 °C, in the temperature range corresponding to the $T_{gel\,max}$ previously determined by both methods, no more association between urea moieties is observed.

We deduced the percentages of free and associated urea by integration of the free amide I band (1694 cm^{-1}) and the associated amide I band (1627 cm^{-1}), assuming that the integrated molar extinction coefficients are constant with the temperature. We investigated the evolution of the ratio between free amide I (% FAI) and associated amide I (% AAI) as a function of the temperature. For each temperature, areas of these two bands can be deduced by deconvolution of FTIR spectra. An example of a deconvoluted FTIR spectrum and area determination of % FAI and % AAI of an organogel of **1** (5 mg mL^{-1}) in tetrachloroethylene at $T = 50$ °C is given in the Supporting Information. From these data, the concentrations of the two species can be calculated and plotted (Figure 2).

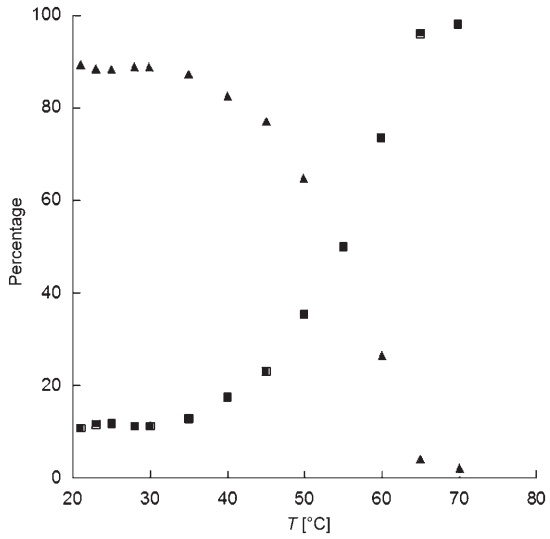

Figure 2. Percentages of free (% FAI, ■) and associated (% AAI, ▲) urea in an organogel of **1** (5 mg mL^{-1}, 0.3 wt %) in tetrachloroethylene as a function of temperature.

The percentage of free urea increases gradually with the temperature. For temperatures close to the T_{gel} (≈50 °C for a 0.3 wt % gel of **1** in C_2Cl_4), the percentage of free urea is about 35 % and the slope of the curve is nearly constant up to 65 °C. At 65 °C, almost all H-bonds are broken. Consistently with the van't Hoff equation, a linear evolution of $\ln K$ as a function of 1/T is found between 30 °C and 50 °C. A ΔH° value of 87 kJ mol^{-1} can be deduced from the slope ($-\Delta H^{\circ}/R$). This value, corresponding to the dissociation of four N–H···O=C hydrogen bonds, is in good agreement with the 46 kJ mol^{-1} reported by Jadzyn et al. for the formation of two N–H···O=C hydrogen bonds in diethylurea.[24] Finally, above T ≈ 65 °C almost all H-bonds are broken and the molecules exist in an isolated state.

From the FTIR study of **1** as an organogel, it is clear that the urea functions play the role of structure directing agents

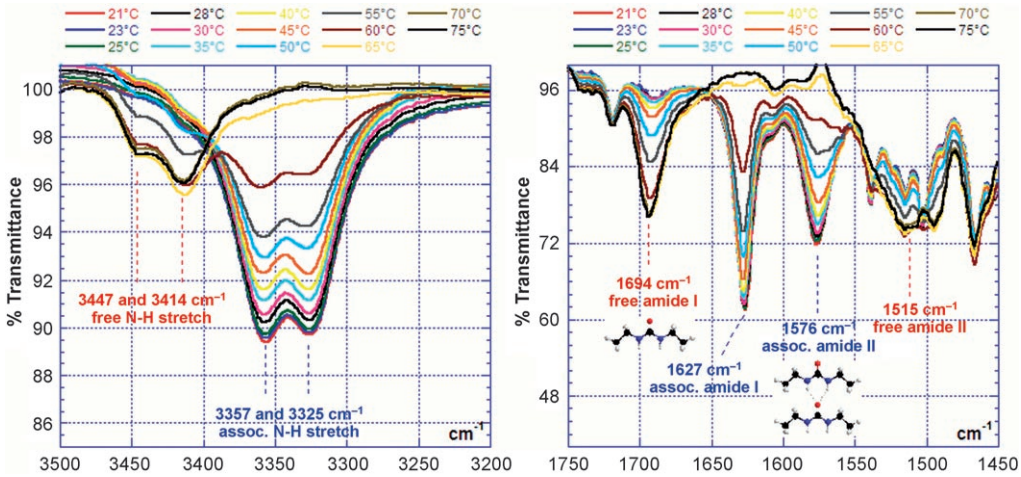

Figure 1. FTIR spectra of an organogel of **1** (5 mg mL^{-1}, 0.3 wt %) in tetrachloroethylene as a function of the temperature.

through hydrogen bonds. The design of the molecule being functionalized by two urea functions should drive the supramolecular organization toward 1D assembly with an optimized overlapping of the π-conjugated segment. In the solid state, the influence of the urea moieties on the supramolecular organization of **1** was revealed by comparison of the optical properties of **1** and **2** (see Supporting Information). Interestingly, the UV/Visible absorbance of **1** was blue-shifted from 413 nm in solution to 406 nm in the solid state, accompanied by a broadening and decrease in intensity of the π–π* absorption bands. These spectral changes can be attributed to a strong exciton coupling between the phenylenethienylene moieties.[10] Apparently, the phenylenethienylene chromophores of **1** are present in the solid state as π-stacked *H*-aggregates.[25] On the other hand, the red shift from 405 to 434 nm observed for **2** suggests a different supramolecular organization with the formation of *J*-aggregates.[26]

The *H*-aggregation of the bisurea deduced from the blue-shifted absorption of its freeze-dried gel was confirmed by study of the emission behavior of the organogelator in tetrachloroethylene as a function of the temperature. An organogel of **1** in tetrachloroethylene (5 mg mL^{-1}) was heated at 115 °C (above the T_{gel}) and irradiated at 400 nm. Emission spectra were recorded during the cooling of the sample (Figure 3).

From Figure 3, two types of spectroscopic behavior can be identified. At 115 °C, **1** exhibits the same emission properties as in dilute solution, with a fluorescence maximum found at 462 nm. The chromophores are perfectly isolated from each other. From 115 to 57 °C, almost no evolution in the shape and the intensity of the spectra is observed. Below 57 °C, a red shift of the emission maximum and a decreased intensity can be seen (see Supporting Information for intermediate temperatures). This transition corresponds to the T_{gel} as already determined by the test tube "tilting" method or by FTIR measurements. Upon aggregation, the strong π–π interaction leads to quenching of emission of individual molecules. In a remarkable way, these spectroscopic phases and their temperatures could be correlated to the hydrogen bond strength and relative orientational transitions of the urea functions determined by FTIR. This spectroscopic behavior observed for **1** upon gelation (blue-shifted absorption, red-shifted and quenched emission) can be attributed to *H*-aggregation,[27,28,29] which is reasonable to expect from an anticipated "card pack" orientation of the phenylenethienylene chromophores in the hydrogen-bonded network directed by the urea.

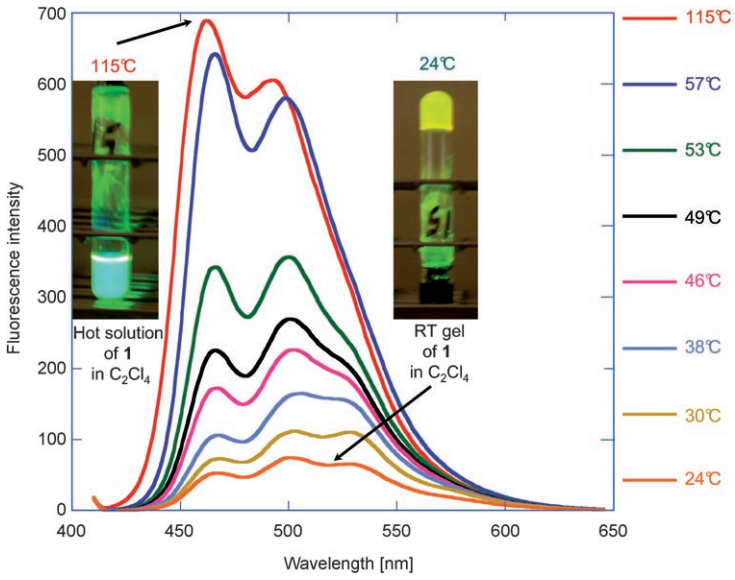

Figure 3. Emission spectra of an organogel of **1** (5 mg mL^{-1}) in tetrachloroethylene irradiated at 400 nm as a function of temperature.

More information about the two different supramolecular organizations exhibited by **1** and **2** was provided by the determination of the crystal structure of **2** (Figure 4a and b). Recrystallization of **2** from acetone furnished orange parallelepipedic single crystals suitable for X-ray diffraction intensity recording on an Xcalibur CCD (Oxford Diffraction) diffractometer. Compound **2** crystallizes in a triclinic system with a $P\bar{1}$ space group. The molecule is located at the inversion centre, and the asymmetric unit is then defined with a half-molecule. As attested to by the crystal structure, the three benzene rings and the two thiophene rings are mostly coplanar, due to the S···O interactions, which favor a small dihedral angle between benzene and thiophene rings and consequently a good π orbital overlap.[13] In the solid state, **2** forms stacks separated by the octyl chains lying perpendicularly to the chromophore long axis (Figure 4a). The interlacing of lateral chains stabilized by van der Waals interactions produces a longitudinal and a lateral slip of the molecules in a given stack toward a *J*-aggregation with a pitch angle of $P_2 = 56°$ and a roll angle of $R_2 = 48°$ (Figure 4b).[30] The pitch and roll angles are used to assess the molecular slipping along the long and the short axes of a molecule. Although the π-stack undergoes a pitch angle distortion of 56°, the molecular π-systems of molecules could still overlap. However with a roll angle distortion of 48°, the adjacent molecules slide completely out from under one another and there is little remaining π-overlap between them.

From the conformation of the π-conjugated core and the lateral aliphatic chains positions obtained from the crystal structure of **2**, and taking into account that bisureas are well known to self-assemble in one-dimensional fashion, it was possible to propose a molecular model (Figure 4c and d).

In that case, both urea groups form hydrogen bonds

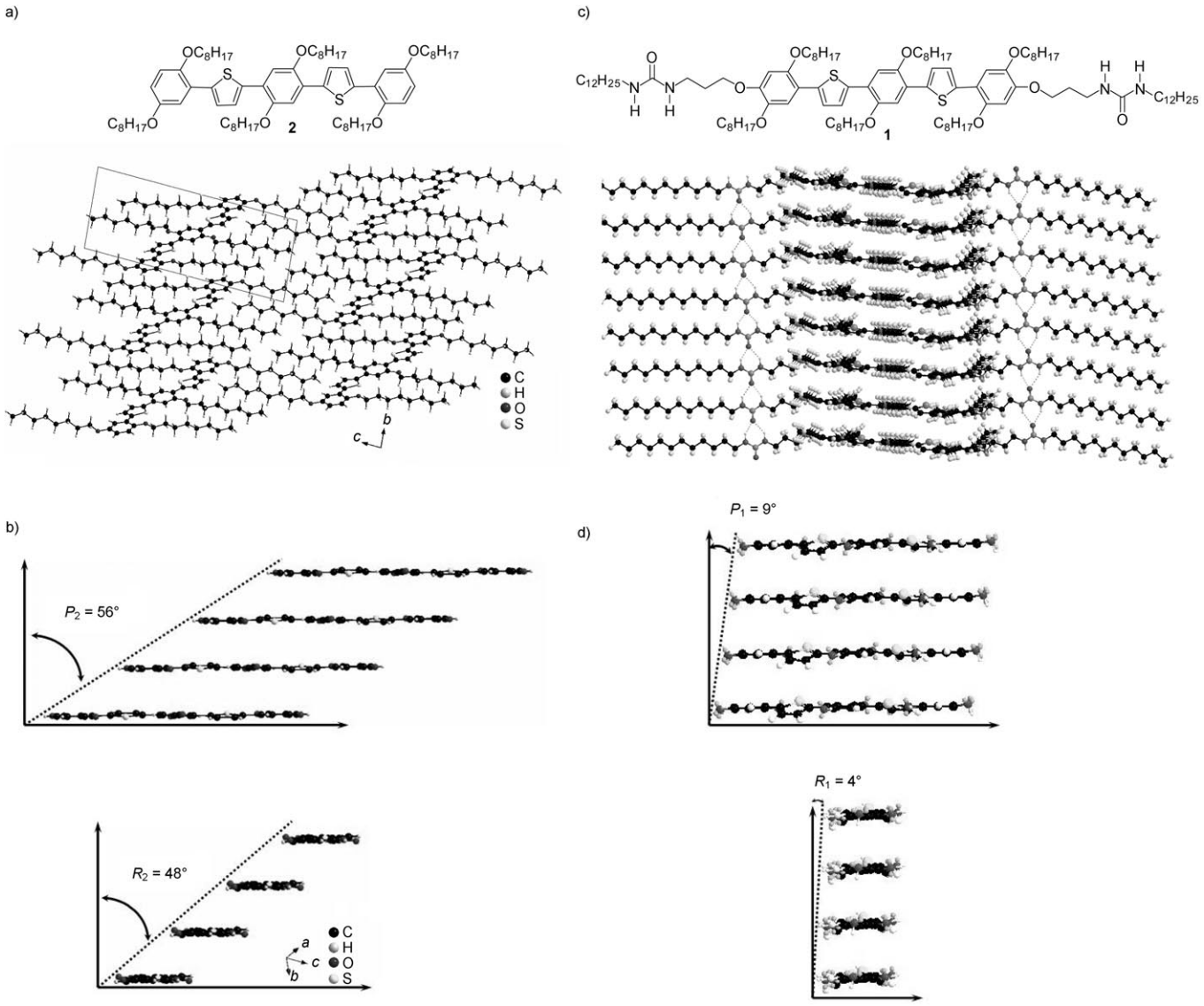

Figure 4. Crystal structure of **2**. a) View of the packing in **2**, as seen down the *a* axis. This illustration shows six molecules, stacked two deep. b) *J* stacks running along the *a* axis (octyl chains have been omitted for clarity) and molecular model proposed for the supramolecular assemblies formed by **1**. c) Infinite chains of hydrogen-bonded urea moieties. d) Face-to face-arrangement of the phenylenethienylene moieties along the same direction as the infinite hydrogen-bonded chains (octyl chains have been omitted for clarity).

with urea groups of neighboring molecules, and thereby participate in the formation of infinite chains of hydrogen-bonded urea moieties (Figure 4c). The average repeat distance along the direction of the hydrogen-bonded chains is 4.5 Å, in accordance with the average value of 4.6 Å found for crystal structures of urea compounds.[31] The phenylenethienylene moieties adopt a face-to-face arrangement along the same direction as the infinite hydrogen-bonded chains (Figure 4d). A modest pitch angle ($P_1 = 9°$) and a very small roll displacement ($R_1 = 4°$) are consistent with an *H*-aggregation in which adjacent molecules of **1** retain appreciable π-overlap.

Shapes of the aggregates: The formation of a gel suggests self-assembly of **1** into nanostructures. Further insight concerning the supramolecular assemblies structuring the organogel was provided by scanning electron microscopy (SEM) and transmission electron microscopy (TEM) images of a freeze-dried gel of **1** (10 $g L^{-1}$ in dichloromethane). As expected, the entire sample is comprised of fiber-like structures with one-dimensional architectures (see Supporting Information).

With the intention of isolating fibers, a gel of **1** (10 $g L^{-1}$) was diluted to 0.5 $g L^{-1}$ in dichloromethane prior to being dropcast on a silicon wafer covered by a dry silicone dioxide film (thickness 250 nm). Atomic force microscopy (AFM) showed an interdigitated network of nanorods formed by association of **1** as a result of hydrogen bonding of urea groups (Figure 5a). When diluted ten times more, however, two different types of nano-objects were obtained, depend-

ing on their location on the substrate. Dispersion of nanorods was found at the periphery of the drop (Figure 5b) whereas nanorings could be observed in the center of the drop (Figure 5c). Sizing of the different nano-objects leads us to postulate two different processes for the formation of the nanorods and the nanorings. Indeed, on the one hand, nanorods obtained after dilution of the gel (Figure 5b) exhibited the same dimensions as those present in the pristine organogel (typical height 4 nm, typical width 70 nm, and typical length 2 μm), suggesting that they had originated from the dispersion of the preexisting nanorods (Figure 5a). On the other hand, the nanorings (Figure 5c) had the same width (70 nm) but much greater height (12 nm). This observation indicates that they are the product of a dewetting process. During the drying of the drop, the concentration of unassociated molecules increases considerably in its center, to form new supramolecular assemblies around nanodrops of solvent or water. Their diameters lie between 200 and 300 nm.

Electrical force microscopy experiments: The electronic behavior of the nano-objects was studied by electrical force microscopy (EFM). We have recently described the use of the EFM technique to study organic nanostructures[32] or DNA samples[33] in previous papers. It is a powerful tool with which to investigate the electrical transport properties of nano-objects. Charge carriers were locally injected by the apex of an atomic force microscope tip, and the resulting distribution and concentration of injected charges were measured by electrical force microscopy (EFM) experiments. The nano-objects were deposited on a highly-doped n-type silicon wafer (resistivity of $\approx 10^{-3}\,\Omega\,cm$), covered by ≈ 4 nm thick thermal oxide grown in dry O_2 at 730 °C. The SiO_2 surface roughness (rms) is ≈ 0.15 nm (AFM measurements). The SiO_2 surfaces were cleaned by a piranha attack and rinsed in deionized water before the nanoring deposition. Local charge injections and EFM experiments were performed with the aid of a Dimension 3100 microscope (Digital Instruments) under air. We used PtIr-coated cantilevers with a free oscillating frequency $f_0 \approx 60$ kHz and a spring constant $k \approx 1$–$3\,N\,m^{-1}$. To inject charges into the nano-object locally, the EFM tip was biased at V_{inj} with respect to the silicon wafer, its oscillation frequency was set to zero, and the tip was gently contacted to the nano-object with a typical 2 nN contact force for two minutes (Figure 6). Image analyses were performed with the DI software or WSxM.[34]

EFM measurements were first carried out on a nanorod measuring 2 μm long, with an average thickness of 2.5 nm and a width of ≈50–100 nm determined by AFM in tapping mode (Figures 5b and 7a). A first EFM image (Figure 7b) was performed before local application of a bias voltage $V_{inj} = +2$ V (i.e., hole injection) over 2 minutes by the apex of the tip. Then, after the hole injection, another EFM image (Figure 7c) was taken under the same scan conditions. It was observed that positive charges (inducing a negative shift of the cantilever frequency biased at $V_{EFM} = -2$ V appearing dark in the EFM image; see below) were delocalized all along the nanorod over micrometers, attesting that molecules inside the nano-objects are reasonably well organized (a more detailed discussion is given below).

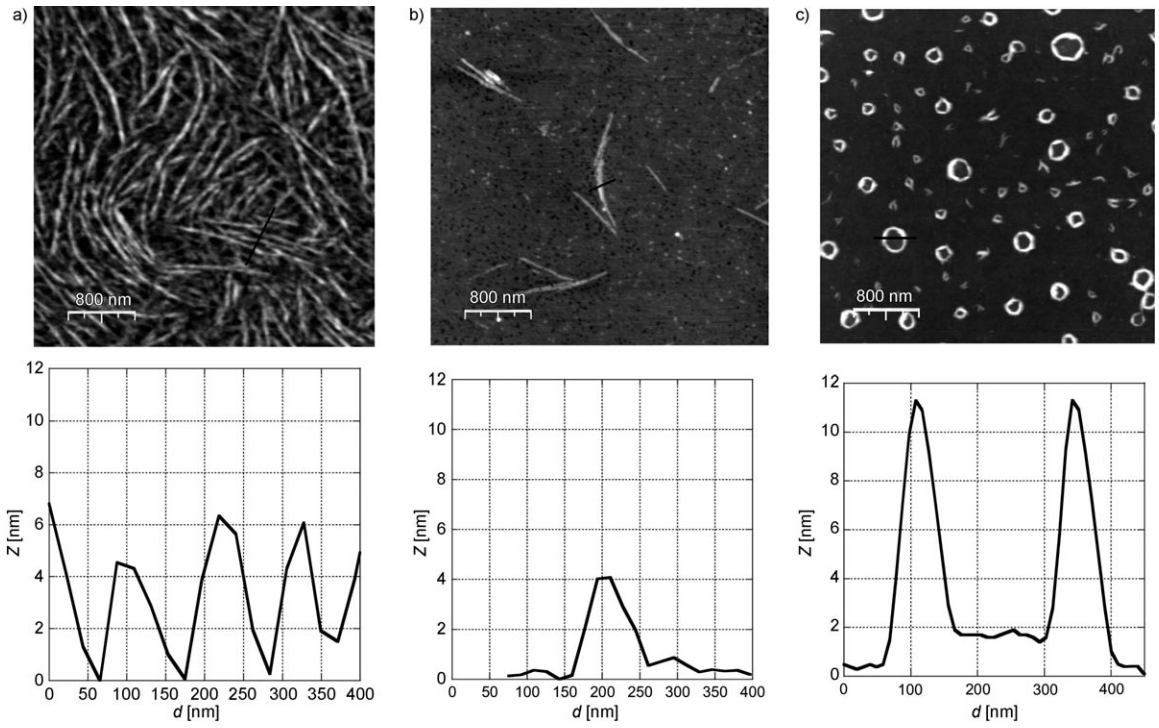

Figure 5. AFM topographic images (taping mode, SiO_2 substrate) and cross-sections (along the black lines) of drop-cast films of the gels of **1** diluted in dichloromethane at: a) 0.5 $g\,L^{-1}$, b) 0.05 $g\,L^{-1}$ periphery of the drop, and c) 0.05 $g\,L^{-1}$ center of the drop.

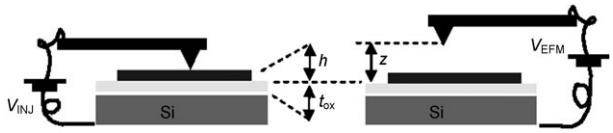

Figure 6. Schematic representation of charge injection and detection by EFM. The silicon substrate is covered by an oxide (thickness t_{ox}—in light grey). The nano-object (in black) has a height h. In the EFM mode, the tip is set at a distance z from the substrate. V_{inj} is the tip bias for injecting charges (electrons at $V_{inj} < 0$, and holes at $V_{inj} > 0$). V_{EFM} is the tip bias for the EFM measurements.

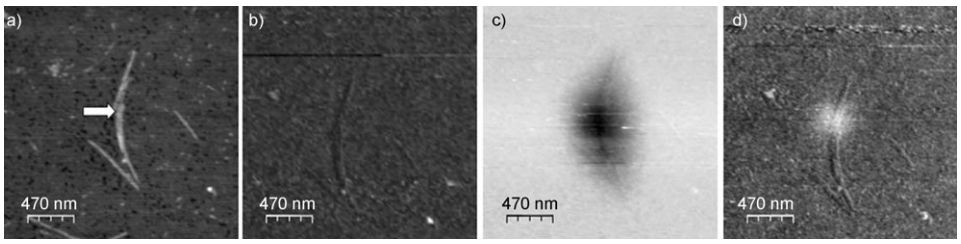

Figure 7. a) Topographic image of a nanorod. b) EFM image before charge injection, c) EFM image after hole injection (at the point marked by the arrow in Figure 7a) in the same nanorod at $V_{inj} = +2$ V for 2 minutes. d) After electron injection at $V_{inj} = -3$ V for 3 min. EFM image conditions: $V_{EFM} = -2$ V, lift $z = 50$ nm.

The distribution of charges injected into the nanorods was characterized by EFM, in which electric force gradients acting on the tip biased at V_{EFM} (here -2 V) shift the EFM cantilever oscillation frequency. For this measurement, the tip–substrate distance was typically $z = 50$ nm (otherwise specified). EFM images are sensitive to two distinct interactions. Firstly, the capacitive interaction associated with the local increase in the tip–substrate capacitance when the EFM tip is moved over the nanorings leads to weak negative frequency shifts, which appear as weak dark features in Figure 7b. The second interaction is the interaction between the charge Q stored in the nanoring and the capacitive charge at the tip apex. This additional frequency shift is either positive or negative, and varies as $Q \times V_{EFM}$. When >0 (repulsive interaction), this corresponds to a positive frequency shift, leading to bright features in the EFM images. In contrast, <0 (attractive interaction) corresponds to a negative frequency shift and thus dark features in the EFM images (as shown in Figure 7c).

A control experiment was performed, in which charges were injected and measured, under the same conditions, directly in the oxide without any nanorod. In that case, the charges stayed localized in the oxide (Figure 8a), and the EFM image showed an isotropic 2D distribution with an average diameter of about 150–200 nm.

To quantify the amount of charge injected into the nanorod, we followed the same protocol as in our recent paper on EFM on pentacene nanostructures,[32] in which the ratio R of the frequency shift Δf_Q due to the charge in the nanoring over the one Δf_C coming from the capacitance effect is related to the surface charge density σ by Equation (1), with ε_0 and ε_R being the vacuum and nanorod permittivity, respectively, e the electron charge, z the tip–substrate distance, V_{EFM} the EFM bias, and V_S the surface potential, which is negligible in our case.[35]

$$R = -\frac{g}{\alpha}\frac{(\sigma/\varepsilon_R)\, e\, z}{\varepsilon_0 (V_{EFM} - V_S)} \quad (1)$$

The factors g and α are two geometric factors associated with the tip and the substrate ($\alpha \approx 1.5$ and $g \approx 3.5$).[32,35,36] The average frequency shifts Δf_C and Δf_Q are estimated from the profile sections of the EFM images before and after injection, respectively (Figure 9). According to Eq. (1), with $\varepsilon_R \approx 3$ (a common value for most organic materials), the maximum charge density is 1.4×10^5 holes μm^{-2}. We observe that this maximum arises at the injection point and that charge density slowly decreases along the nanorods.

We also note (Figure 7c) that the EFM signal extends widely over the nanorod in the perpendicular direction (≈500 nm on each side). This cannot be explained by convolution with the tip size and shape (radius of 15–20 nm), nor by the intrinsic spatial resolution of the EFM (≈50 nm under our experimental conditions).[37] In the present case, this also cannot be explained by charge injection into the oxide through the nanorod, because the blank experiment (Figure 8a) shows that charge injected (under the same conditions) into the oxide spreads over a smaller distance. While it is likely that charges have also been injected into the oxide (as in our previous experiments on pentacene monolayer islands),[32] we surmise that charges can also spread away from the nanorod as a result of the presence of residual organic materials left on the substrate by the dipping process. To test this hypothesis, we injected holes under the same conditions into the oxide substrate, away from a nanorod (Figure 8b). We clearly observed an isotropic diffu-

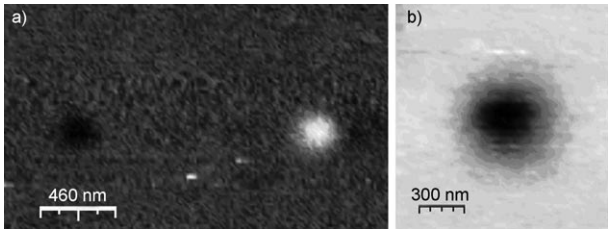

Figure 8. a) EFM image of charges (electrons at $V_{inj} = -2$ V (right hand-side) and holes at $V_{inj} = +2$ V (left hand-side)) directly injected into the naked 4 nm thick SiO_2 layer (as grown oxide). b) EFM image of hole injection under the same conditions as in Figure 7c ($V_{inj} = +3$ V for 2 minutes) in the oxide, away from the nanorod, after the nanorod deposition process. All EFM image conditions: $V_{EFM} = -2$ V, lift $z = 50$ nm.

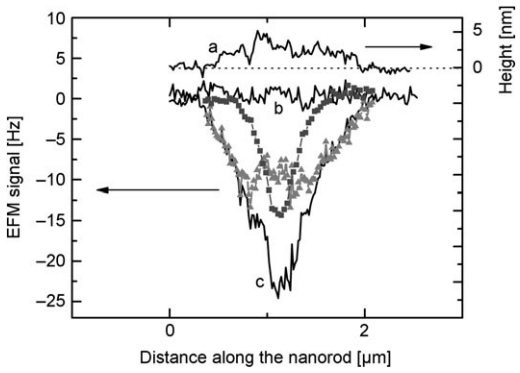

Figure 9. Topographic (a) and EFM (b–c) profiles along the nanorods. The profiles are taken along a curved line following the long axis of the nanorods. b) EFM before hole injection and c) after hole injection (same conditions as in Figure 7). EFM profile (■) for hole injection in the oxide substrate after the deposition of the nanorods (from Figure 8b), net EFM signal due to charges in the nanorod (▲) obtained by subtracting the oxide contribution (■) from the measured profile after injection (curve c).

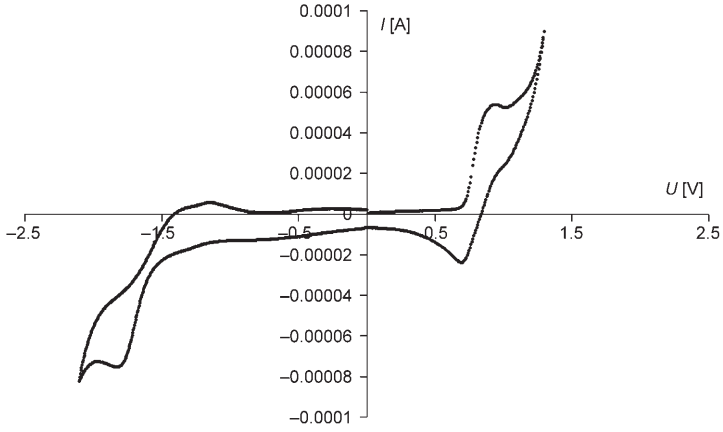

Figure 10. Cyclic voltammogram of a solution of **1** in THF (10^{-3} mol L^{-1}) containing Bu_4NPF_6 (0.1 mol L^{-1}) as a supporting electrolyte at a scan rate of 100 mV s^{-1}, referenced vs. SCE.

sion of charges, as in the naked substrate (Figure 8a), but with a larger diffusion distance ($\approx$1 μm).[38] The corresponding EFM profile is also shown in Figure 9 (line with squares). To distinguish the respective contributions of charge in the nanorod and in the oxide substrate in Figures 7c and 9c, this oxide contribution is subtracted from the raw EFM profile shown in Figure 9c. The resulting EFM signal due to the net charges in the nanorod is shown by the line with triangles in Figure 9. We can conclude that the injected holes in the nanorod are almost homogeneously spread along the nanorod over a distance of $\approx$1 μm, and that their density slowly decreases near the edges. The EFM plateau at ≈ -10 Hz corresponds to $\approx 5.8\times10^4$ holes μm^{-2}.

The same experiments with negative bias (i.e., electron injection) were carried out, but no charge delocalization was noted (Figure 7d). We only observed a weak bright isotropic spot (diameter of about 250–300 nm). By comparison with the blank experiment (Figure 8a), this probably corresponds to electron injection into the oxide underneath.

These results could be correlated with electrochemical measurements performed on **1**. Figure 10 shows a full-scan cyclic voltammogram of a solution of **1** in THF (10^{-3} mol L^{-1}) containing Bu_4NPF_6 (0.1 mol L^{-1}) as a supporting electrolyte. At a scan rate of 100 mV s^{-1} referenced vs. SCE, **1** exhibits an irreversible wave under cathodic sweep and the reduction takes place at −1.56 V vs. SCE. The oxidation process exhibits a pseudo-reversible wave when swept anodically, and the onset potential of oxidation for **1** is located at 0.63 V vs. SCE. Thus, it is easier to inject holes into the HOMO of **1**, which is a good electron-donor, than to inject electrons in the LUMO.

Further experiments were performed on the nanorings shown in Figure 5c. Figure 11a and c show the topographic images before and after the charge injection (done at the point marked by an arrow). By comparing the two images, we checked that the injection protocol had not deformed the nanoring. Figure 11b and d represent the EFM images before and after hole injection at $V_{inj}=+2$ V for 2 min. It is clear that the injected holes have been delocalized along the nanoring, while more charges have been injected in the right-hand part of the nanoring close to the injection point. It is also clear that some charges have spread away from the nanoring due to the presence of residual materials on the substrate around the nanoring (as clearly shown in the topographic image).

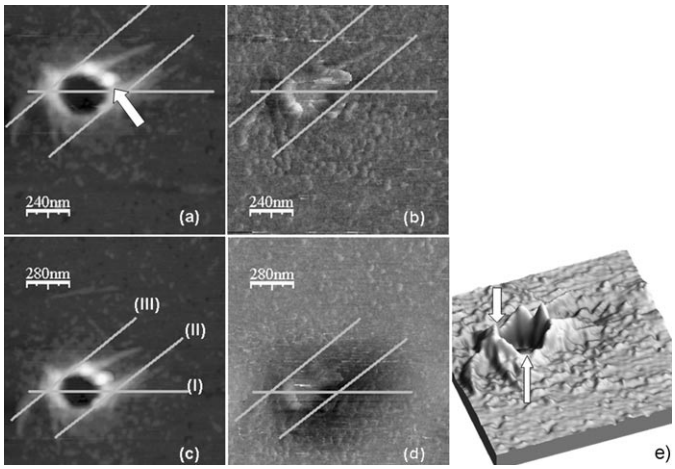

Figure 11. a) and c) Topographic images of the nanoring before and after hole injection at $V_{inj}=+2$ V over 2 min at the point indicated by the arrow. b) and d) Corresponding EFM images recorded at $V_{EFM}=-2$ V and $z=50$ nm. e) 3D topographic image (from a) showing two constrictions marked by the arrows.

Figure 12 shows three different profiles of the nanoring taken along the lines I, II, and III (as shown in Figure 11), before (in blue) and after (in red) hole injections (topographic profiles are also shown along the same lines). From these EFM profiles, and by using $\varepsilon R\approx 3$ (a common value for organic materials), we can deduce[39] that $\approx$1.8–2.1×

10^4 holes μm^{-2} have been injected into the right-hand part of the nanoring (profiles I and II) and $\approx 7.5 \times 10^3$ holes μm^{-2} into the left-hand part (profile III). In view of the shape and size of the nanoring (Figure 11 and topographic profile along I in Figure 12), with an internal radius of $\approx$50 nm and an external radius of $\approx$250 nm, these values correspond to ≈ 3.3–4.2×10^3 and $\approx 1.5 \times 10^3$ holes, respectively. The fact that fewer charges have been delocalized on the left-hand side of the nanoring may be related to the presence of "defects". From the 3D image (Figure 11e), we can observe two constrictions (shown by the arrows) in the nanoring, separating its left- and right-hand parts. These constrictions partly prevent the diffusion of charge from the right-hand part of the nanoring to the left.

Other experiments on nanorings without defects (Figure 13a) showed a more uniform charge distribution all over the nanoring (Figure 13b and c).

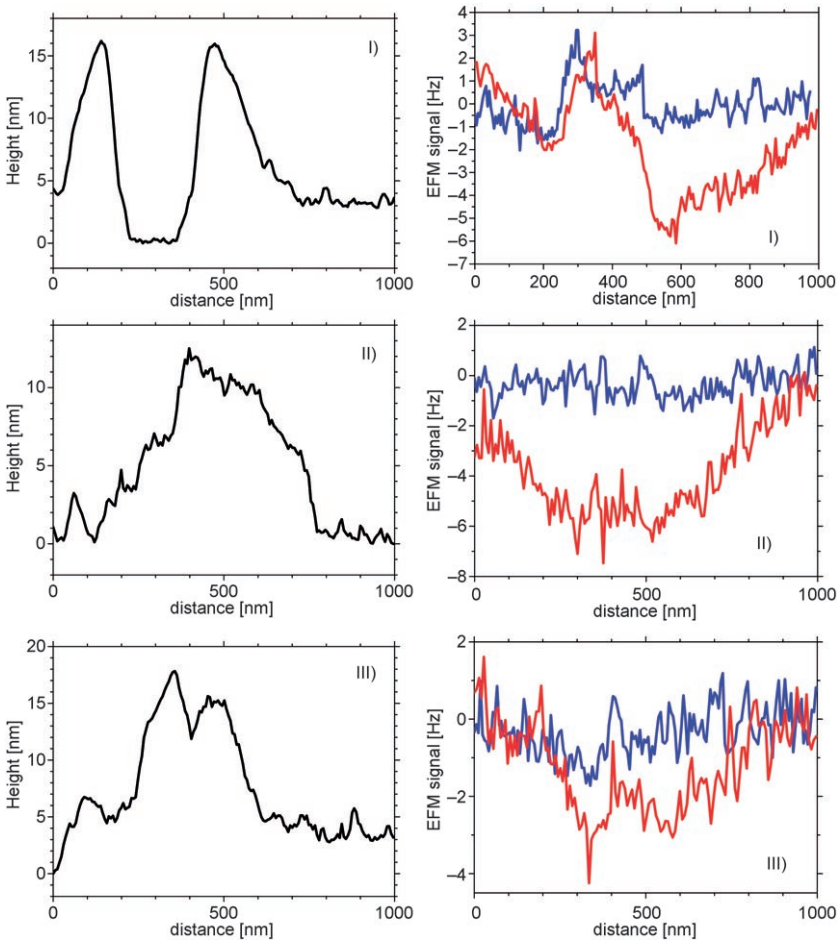

Figure 12. Profiles along the lines I, II and III as shown in Figure 11. Left-hand images: AFM heights. Right-hand images: EFM frequency shift measured before the hole injection (blue, from EFM image in Figure 11b) and after the hole injection (red, from EFM image in Figure 11d).

Conclusion

In summary, we have synthesized a π-conjugated oligo(phenylenethienylene) capable of forming one-dimensional supramolecular assemblies, leading to gelation of several solvents. From the FTIR study of **1** as an organogel, it was shown that the urea functions play the role of structure directing agents through hydrogen bonds. The *H*-aggregation of the bisurea deduced from the blue-shifted absorption of its freeze-dried gel was confirmed by the study of the emission behavior of the organogelator in tetrachloroethylene as a function of temperature. As suggested by the formation of an organogel, supramolecular architectures were imaged by scanning electron microscopy of a freeze-dried gel. As expected, the entire sample is comprised of fiber-like structures with one-dimensional architectures. Nano-objects were successfully isolated under special conditions of dilution of the organogel. Two different types of nano-objects were obtained, depending on their location on the substrate. A dispersion of nanorings was found in the center of the drop, whereas nanorods could be observed at the pe-

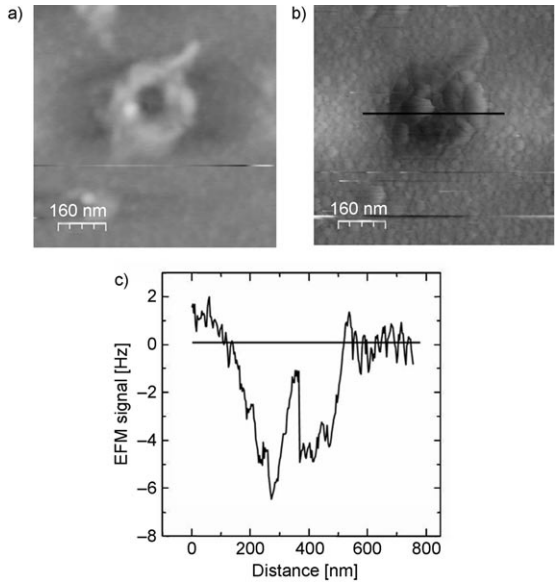

Figure 13. a) Topographic and b) EFM image of a defect-free nanoring. c) EFM profile along the line in b). Hole injection and EFM conditions as in Figure 11.

riphery. Sizing of the different nano-objects leads us to postulate two different processes for the formation of the nanorods and the nanorings. Isolated nanorods are certainly the result of the dispersion of preexisting nanorods, while nanorings could be the product of a dewetting process. Their electronic properties such as positive charges transport have been demonstrated by the EFM technique. It was observed that positive charges were nonuniformly delocalized all along an isolated nano-object over micrometers. In particular, no charge was stored in the centers of the nanorings. The observed negative frequency shift corresponds to about $1.5–4\times10^3$ injected charges in the nanoring. The same experiments have been performed with negative bias (i.e., electrons injection), but no charge delocalization was noted. These results could be correlated with the nature of **1**, which is a good electron-donor, so it can be easily oxidized, but reduced only with difficulty. It was observed that topographic constrictions in the nanostructures prevent the charge transport and delocalization. Organic nanorings could be very interesting for persistent-current experiments.[40]

Experimental Section

General information and techniques: All synthetic experiments were performed under nitrogen by conventional Schlenk line techniques. The reagents 2,5-dioctyloxyphenyleneboronic acid,[41] 1,4-dioctyloxybenzene (**3**),[16] 2,5-dioctyloxy-1,4-phenylenediboronic acid,[16] and 1,4-bis(2′-thienyl)-2,5-dioctyloxybenzene[42] were prepared by known procedures. 2,5-Dioctyloxyphenol (**5**) was prepared by our modification of the protocol described in References [16] and [17]. The analytical data for **5** were in good accordance with the literature. *N*-(3-Bromopropyl)phthalimide, 1-dodecyl isocyanate, and thiophene-2-boronic acid were purchased from Acros, *N*-bromosuccinimide (NBS) and *N*-iodosuccinimide (NIS) from Alfa Aesar. Dichloromethane was distilled over CaH_2, THF over $LiAlH_4$ then sodium/benzophenone under nitrogen. Melting points were determined on an electrothermal apparatus (IA9000 series) and are uncorrected. ^{1}H and ^{13}C NMR spectra in solution were recorded on Bruker AC 200 and AC 250 spectrometers at room temperature with deuterated chloroform for solvent and TMS as internal reference. IR data were obtained on a Perkin–Elmer 1000 FT-IR spectrophotometer. Mass spectra were measured on JEOL MS-SX 102 and Autospec EQ mass spectrometers. SEM images were obtained with JEOL 6300 F microscopes.

1,4-Bis(5-bromothien-2-yl)-2,5-dioctyloxybenzene: 1,4-Bis(thien-2-yl)-2,5-dioctyloxybenzene (1.5 g, 3 mmol) was added to a solution of NBS (1.1 g, 6.2 mmol) in dichloromethane (30 mL). The mixture was then stirred for 5 h. After aqueous workup the solvent was removed under vacuum to yield a yellow powder, which was purified by flash chromatography (silica gel, gradient of cyclohexane/dichloromethane) (1.7 g, 2.7 mmol, 89 %). M.p. 89 °C; ^{1}H NMR (200 MHz, $CDCl_3$): $\delta=7.22$ (d, $^3J(H,H)=3.9$ Hz, 2H), 7.09 (s, 2H), 7.03 (d, $^3J(H,H)=3.9$ Hz, 2H), 4.01 (t, $^3J(H,H)=6.5$ Hz, 4H), 1.90 (m, 4H), 1.20–1.65 (m, 20H), 0.89 ppm (m, 6H); ^{13}C NMR (50 MHz, $CDCl_3$): $\delta=148.9$, 140.4, 129.2, 124.5, 122.4, 113.1, 111.1, 69.8, 31.9, 29.42, 29.4, 26.3, 22.7, 14.2 ppm; IR (KBr): $\tilde{\nu}=$ 3084, 2944, 2919, 2867, 2848, 1537, 1491, 1462, 1210, 1064, 786 cm^{-1}; HRMS (FAB+): *m*/*z*: calcd for $C_{30}H_{40}Br_2O_2S_2$: 654.0836 $[M]^+$; found: 654.0833.

1,4-Bis[5-(2,5-dioctyloxyphenyl)thien-2-yl]-2,5-dioctyloxybenzene (2): A mixture of 1,4-bis(5-bromothien-2-yl)-2,5-dioctyloxybenzene (520 mg, 0.8 mmol), 2,5-dioctyloxyphenylboronic acid (640 mg, 1.6 mmol), K_3PO_4 (1 g, 4.8 mmol), Pd_2dba_3 (35 mg, 35 μmol), and triphenylphosphine (35 mg, 280 μmol) in DMF (40 mL) was heated under nitrogen at 80 °C for 3 days. The DMF was then evaporated. After aqueous workup and extraction of the product with dichloromethane, a brown solid was obtained and purified by column chromatography (silica gel, gradient of cyclohexane/dichloromethane) to yield an orange powder (260 mg, 0.2 mmol, 28 %). M.p. 88 °C; ^{1}H NMR (200 MHz, $CDCl_3$): $\delta=7.52$ (m, 4H), 7.26 (m, 4H), 6.89 (dd, $^3J(H,H)=8.8$, $^4J(H,H)=2.4$ Hz, 2H), 6.77 (d, $^3J(H,H)=3.9$ Hz, 2H), 1.70–2.00 (m, 12H), 4.01 (m, 12H), 1.20–1.65 (m, 60H), 0.88 ppm (m, 18H); ^{13}C NMR (50 MHz, $CDCl_3$): $\delta=153.2$, 149.6, 149.5, 139.3, 125.8, 125.6, 124.6, 123.2, 114.4, 114.2, 113.9, 112.9, 69.7, 68.7, 31.8, 29.4, 29.4, 29.2, 26.2, 26.2, 26.1, 22.6, 14.1 ppm; IR (KBr): $\tilde{\nu}=3082$, 2952, 2923, 2868, 2852, 1603, 1535, 1497, 1466, 1221, 800 cm^{-1}; elemental analysis (%) calcd for: C 76.37, H 9.87, O 8.25; found: C 75.93, H 9.80, O 8.17.

1-(2,5-Dioctyloxyphenyl)ethan-1-one (4): 1,4-Dioctyloxybenzene (**3**, 20.4 g, 60.9 mmol) and acetyl chloride (2 equiv, 9.7 g, 138.8 mmol) were mixed in CCl_4 (75 mL) at 5 °C. $AlCl_3$ (1.2 equiv, 9.7 g, 73.2 mmol) was then carefully added to this yellow solution by spatula in small portions over 30 min. After the addition, the dark red solution was heated to room temperature for 16 h and became black. During the reaction HCl was released; the acidic overpressure was neutralized by bubbling through a KOH solution. The medium was quenched with a water/ice mixture, and the organic layer was washed three times with water, dried over Na_2SO_4, and filtered, and the solvent was removed under vacuum. The product was purified by column chromatography (silica gel, gradient of pentane/dichloromethane 10:0 → 7:3). Compound **4** was isolated as a white solid (19.3 g, 51.3 mmol, 85 %). ^{1}H NMR (200 MHz, $CDCl_3$): $\delta=$ 7.28 (d, $^4J(H,H)=3.1$ Hz, 1H; Ar), 6.99 (dd, $^3J(H,H)=9.1$, $^4J(H,H)=$ 3.1 Hz, 1H; Ar), 6.85 (d, $^3J(H,H)=9.1$ Hz, 1H; Ar), 3.98 (d, $^3J(H,H)=$ 6.5 Hz, 2H; OCH_2), 3.91 (d, $^3J(H,H)=6.5$ Hz, 2H; OCH_2), 2.62 (s, 3H; CH_3), 1.90–1.65 (m, 4H), 1.55–1.35 (m, 4H), 1.28 (brs, 16H), 0.95–0.80 ppm (m, 6H).

2,5-Dioctyloxyphenol (5): A solution of peracetic acid in AcOEt (61 %, 2 equiv, 17.0 mL, 102.6 mmol) was slowly added over 30 min at 40 °C to a solution of **4** (19.9 g, 51.2 mmol) in AcOEt (15 mL). The brownish solution turned reddish and was stirred for an additional 16 h. The crude product was washed with brine (150 mL), and the aqueous layer was extracted twice with AcOEt. The organic layers were combined, washed once with H_2O, dried over Na_2SO_4, and filtered, and the solvent was carefully removed under vacuum. KOH (4 equiv, ≈0.2 mol) and EtOH (2 equiv, ≈0.1 mol) were mixed with the crude product in water (50 mL), and the mixture was heated to 80 °C and stirred for 1 h 30. The solution was then cooled to −30 °C, and HCl (1.5 N, ca 0.2 mol) was added (pH < 2). The organic layer was washed twice with brine, dried over Na_2SO_4, and filtered through Celite, and the solvent was removed under vacuum. The product was recrystallized from MeOH at −30 °C. Compound **5** was isolated as a white solid (14.4 g, 41.1 mmol, 80 %). M.p. 5 °C; ^{1}H NMR (200 MHz, $CDCl_3$): $\delta=6.74$ (d, $^3J(H,H)=8.8$ Hz, 1H; Ar), 6.55 (d, $^4J(H,H)=2.9$ Hz, 1H; Ar), 6.35 (dd, $^3J(H,H)=8.8$, $^4J(H,H)=2.9$ Hz, 1H; Ar), 4.9 (brs, 1H; OH), 3.96 (d, $^3J(H,H)=6.5$ Hz, 2H; OCH_2), 3.87 (d, $^3J(H,H)=6.6$ Hz, 2H; OCH_2), 1.85–1.65 (m, 4H), 1.60–1.35 (m, 4H), 1.29 (brs, 16H), 0.95–0.85 ppm (m, 6H); ^{13}C NMR (50 MHz, $CDCl_3$): $\delta=$ 153.9, 146.6, 140.1, 112.7, 105.1, 102.2, 69.7, 68.4, 32.5, 31.7, 29.3, 29.2, 29.1, 26.0, 25.9, 22.6, 14.0 ppm.

***N*-[3-(2,5-Dioctyloxyphenoxy)propyl]phthalimide (6)**: Compound **5** (1.48 g, 4.2 mmol) was added to a solution of *N*-(3-bromopropyl)phthalimide (1.13 g, 4.2 mmol) and K_2CO_3 (0.88 g, 6.3 mmol) in acetonitrile (50 mL). The mixture was then stirred for 2 days. After aqueous workup and extraction of the product with dichloromethane, a dark brown oil was obtained and purified by column chromatography (silica gel, gradient of cyclohexane/dichloromethane) to yield a white powder (1.64 g, 3.3 mmol, 72 %). M.p. 91 °C; ^{1}H NMR (250 MHz, $CDCl_3$): $\delta=7.76$ (m, 4H), 6.77 (d, $^3J(H,H)=8.9$ Hz, 1H), 6.48 (d, $^4J(H,H)=2.8$ Hz, 1H), 6.37 (dd, $^3J(H,H)=8.9$, $^4J(H,H)=2.8$ Hz, 1H), 4.03 (t, $^3J(H,H)=6.1$ Hz, 2H), 3.87 (m, 6H), 2.20 (m, 2H), 1.73 (m, 4H), 1.2–1.5 (m, 20H), 0.88 ppm (m, 6H); ^{13}C NMR (50 MHz, $CDCl_3$): $\delta=168.2$, 154.1, 150.0, 143.4, 133.8, 132.2, 123.2, 116.1, 105.3, 103.2, 70.6, 68. 4, 66.8, 35.3, 31.8, 29.5, 29.4, 29.2, 29.2, 28.6, 26.1, 26.0, 22.6, 14.0 ppm; IR (KBr): $\tilde{\nu}=3076$, 2940, 2869, 2854, 1773, 1712, 1226, 722 cm^{-1}; HRMS (FAB+): *m*/*z*: calcd for $C_{33}H_{47}NO_5$: 537.3454 $[M]^+$; found: 537.3448.

***N*-[3-(4-Iodo-2,5-dioctyloxyphenoxy)propyl]phthalimide (7)**: Compound **6** (1.02 g, 1.89 mmol) was added to a solution of NIS (0.45 g, 1.99 mmol) and trifluoroacetic acid (65 mg, 0.6 mmol) in dichloromethane (40 mL). The mixture was then stirred for 2 h. After aqueous workup and extraction of the product with dichloromethane, the solvent was removed under vacuum to yield a yellow powder (1.2 g, 1.8 mmol, 94%). M.p. 86°C; ^{1}H NMR (250 MHz, $CDCl_3$): δ = 7.77 (m, 4H), 7.20 (s, 1H), 6.49 (s, 1H), 4.05 (t, ^3J(H,H) = 5.6 Hz, 2H), 3.87 (m, 6H), 2.20 (m, 2H), 1.73 (m, 4H), 1.2–1.5 (m, 20H), 0.88 ppm (m, 6H); ^{13}C NMR (50 MHz, $CDCl_3$): δ = 168.2, 152.7, 149.9, 144.6, 133.9, 132.1, 125.1, 123.2, 102.4, 75.5, 10.5, 70.3, 67.6, 35.3, 31.8, 29.3, 29.2, 28.6, 26.1, 26.0, 22.6, 14.1 ppm; IR (KBr): $\tilde{\nu}$ = 3058, 2948, 2921, 2866, 2852, 1772, 1710, 1213, 710 cm^{-1}; HRMS (FAB+): *m*/*z*: calcd for $C_{33}H_{46}NO_5$: 663.2421 $[M]^+$; found: 663.2448.

***N*-[3-(4-Thienyl-2,5-dioctyloxyphenoxy)propyl]phthalimide (8)**: A mixture of **7** (1.1 g, 1.73 mmol), thiophene-2-boronic acid (330 mg, 2.60 mmol), Na_2CO_3 (400 mg, 3.46 mmol), Pd_2dba_3 (36 mg, 36 μmol), and triphenylphosphine (36 mg, 285 μmol) in THF (20 mL) and water (10 mL) was heated under nitrogen at 50°C overnight. The THF was then evaporated. After aqueous workup and extraction of the product with dichloromethane, a brown solid was obtained and purified by column chromatography (silica gel, gradient of cyclohexane/dichloromethane) to yield a white powder (760 mg, 1.2 mmol, 71%). M.p. 93°C; ^{1}H NMR (250 MHz, $CDCl_3$): δ = 7.77 (m, 4H), 7.37 (dd, ^3J(H,H) = 3.7, ^4J(H,H) = 1.1 Hz, 1H), 7.25 (dd, ^3J(H,H) = 5.3, ^4J(H,H) = 1.1 Hz, 1H), 7.04 (dd, ^3J(H,H) = 5.3, ^3J(H,H) = 3.7 Hz, 1H), 7.02 (s, 1H), 6.59 (s, 1H), 4.10 (t, ^3J(H,H) = 5.9 Hz, 2H), 3.95 (m, 6H), 2.21 (m, 2H), 1.82 (m, 4H), 1.2–1.5 (m, 20H), 0.88 ppm (m, 6H); ^{13}C NMR (50 MHz, $CDCl_3$): δ = 168.2, 150.0, 149.1, 143.5, 139.6, 133.8, 132.2, 126.5, 124.4, 124.0, 123.2, 116.5, 115.8, 102.2, 70.7, 69.7, 67.6, 35.4, 31.1, 29.5, 29.4, 29.3, 29.2, 29.2, 28.7, 26.2, 26.0, 22.6, 14.2 ppm; IR (KBr): $\tilde{\nu}$ = 3068, 2939, 2923, 2870, 2855, 1770, 1706, 1216, 721 cm^{-1}; HRMS (FAB+): *m*/*z*: calcd for $C_{37}H_{49}NO_5S$: 619.3331 $[M]^+$; found: 619.3320.

***N*-[3-(4-(5-iodothiophen-2-yl)-2,5-dioctyloxyphenoxy)propyl]phthalimide (9)**: Compound **8** (300 mg, 0.48 mmol) was added to a solution of NIS (110 mg, 0.48 mmol) in dichloromethane (15 mL). The mixture was then stirred for 2 h. After aqueous workup and extraction of the product with dichloromethane, the solvent was removed in vacuum to yield a yellow powder (350 mg, 0.45 mmol, 89%). M.p. 84°C; ^{1}H NMR (250 MHz, $CDCl_3$): δ = 7.77 (m, 4H), 7.20 (d, ^3J(H,H) = 3.2 Hz, 1H), 7.13 (s, 1H), 7.05 (d, ^3J(H,H) = 3.2 Hz, 1H), 6.59 (s, 1H), 4.12 (t, ^3J(H,H) = 5.0 Hz, 2H), 4.03 (t, ^3J(H,H) = 5.3 Hz, 2H), 3.95 (t, ^3J(H,H) = 5.4 Hz, 4H), 2.23 (m, 2H), 1.90 (m, 2H), 1.77 (m, 2H), 1.2–1.5 (m, 20H), 0.88 ppm (m, 6H); ^{13}C NMR (50 MHz, $CDCl_3$): δ = 168.2, 149.8, 149.5, 143.5, 133.8, 132.2, 124.4, 123.2, 115.7, 114.8, 101.8, 73.0, 70.7, 69.8, 67.5, 35.3, 31.8, 29.5, 29.3, 29.2, 28.6, 26.2, 26.0, 22.6, 14.0 ppm; IR (KBr): $\tilde{\nu}$ = 3059, 2951, 2925, 2868, 2851, 1770, 1706, 1216, 720 cm^{-1}; HRMS (FAB+): *m*/*z*: calcd for $C_{37}H_{49}NO_5S$: 745.2298 $[M]^+$; found: 745.2463.

1,4-Bis[5-(4-(3-phthalimid-*N*-yl)propoxy)-2,5-dioctyloxyphenyl)thien-2-yl]-2,5-dioctyloxybenzene (10): A mixture of **8** (540 mg, 0.73 mmol), 2,5-dioctyloxy-1,4-phenylenediboronic acid (212 mg, 0.36 mmol), Na_2CO_3 (150 mg, 1.44 mmol), Pd_2dba_3 (15 mg, 15 μmol), and triphenylphosphine (15 mg, 120 μmol) in THF (25 mL) and water (5 mL) was heated under nitrogen at 50°C overnight. The THF was then evaporated. After aqueous workup and extraction of the product with dichloromethane, a dark brown solid was obtained and purified by column chromatography (silica gel, gradient of cyclohexane/dichloromethane) to yield a orange powder (300 mg, 0.19 mmol, 53%). M.p. 119°C; ^{1}H NMR (250 MHz, $CDCl_3$): δ = 7.79 (m, 8H), 7.45 (d, ^3J(H,H) = 3.8 Hz, 2H), 7.42 (d, ^3J(H,H) = 3.8 Hz, 2H), 7.26 (s, 2H), 7.23 (s, 2H), 6.64 (s, 2H), 3.80–4.20 (m, 20H), 2.25 (m, 4H), 1.94 (m, 8H), 1.79 (m, 4H), 1.2–1.5 (m, 60H), 0.88 ppm (m, 18H); ^{13}C NMR (50 MHz, $CDCl_3$): δ = 168.3, 150.1, 149.5, 149.0, 143.6, 139.5, 138.3, 133.9, 132.2, 125.5, 124.6, 123.2, 123.1, 116.9, 115.5, 112.8, 102.4, 70.6, 69.8, 69.7, 67.6, 35.4, 31.8, 29.6, 29.29.4, 29.4, 29.3, 28.7, 26.2, 26.1, 22.7, 14.1 ppm; IR (KBr): $\tilde{\nu}$ = 3054, 2951, 2924, 2868, 2853, 1773, 1715, 1213, 719, 711 cm^{-1}; HRMS (FAB+): *m*/*z*: calcd for $C_{96}H_{133}N_2O_{12}S_2$: 1569.9299 $[M+H]^+$; found: 1569.9289.

1,4-Bis[5-(4-(3-aminopropoxy)-2,5-dioctyloxyphenyl)thien-2-yl]-2,5-dioctyloxybenzene (11): Hydrazine monohydrate (1 mL) was added to a solution of **10** (200 mg, 0.12 mmol) in THF (10 mL). The mixture was then stirred at 50°C overnight. After workup with aqueous sodium hydroxide (1 N) and extraction of the product with dichloromethane, a bright yellow powder (150 mg, 0.11 mmol, 96%) was obtained. M.p. 122°C; ^{1}H NMR (250 MHz, $CDCl_3$): δ = 7.45 (d, ^3J(H,H) = 3.9 Hz, 2H), 7.42 (d, ^3J(H,H) = 3.9 Hz, 2H), 7.26 (s, 2H), 7.23 (s, 2H), 6.61 (s, 2H), 3.90–4.20 (m, 16H), 2.96 (t, ^3J(H,H) = 6.7 Hz, 4H), 1.80–2.10 (m, 16H), 1.2–1.5 (m, 64H), 0.88 ppm (m, 18H); ^{13}C NMR (50 MHz, $CDCl_3$): δ = 150.1, 149.5, 148.2, 143.3, 139.6, 138.2, 125.5, 124.6, 123.1, 116.4, 115.0, 112.8, 101.5, 70.4, 69.9, 69.7, 67.9, 39.5, 33.1, 31.8, 29.6, 29.5, 29.5, 29.4, 29.3, 28.7, 26.2, 26.1, 22.7, 14.1 ppm; IR (KBr): $\tilde{\nu}$ = 3390, 3054, 2952, 2924, 2868, 2854, 1210, 794 cm^{-1}; HRMS (FAB+): *m*/*z*: calcd for $C_{80}H_{128}N_2O_8S_2$: 1309.9190 $[M+H]^+$; found: 1309.9210; elemental analysis (%) calcd for: C 73.43, H 8.47, N 1.78, S 4.08; found: C 73.13, H 8.55, N 1.86, S 4.42.

1,4-Bis[5-(4-(3-dodecylureidopropoxy)-2,5-dioctyloxyphenyl)thien-2-yl]-2,5-dioctyloxybenzene (1): 1-Dodecyl isocyanate (60 mg, 0.27 mmol) was added under nitrogen to a solution of **11** (160 mg, 0.12 mmol) in dry THF (20 mL). The mixture was then stirred for 2 h. The solvent was evaporated, and the yellow precipitate was washed several times with pentane (155 mg, 89 μmol, 73%). M.p. 145°C; ^{1}H NMR (250 MHz, $CDCl_3$): δ = 7.52 (d, ^3J(H,H) = 3.9 Hz, 2H), 7.40 (d, ^3J(H,H) = 3.9 Hz, 2H), 7.26 (s, 2H), 7.23 (s, 2H), 6.58 (s, 2H), 5.17 (m, 2H), 4.41 (m, 2H), 4.00–4.20 (m, 16H), 3.45 (m, 4H), 3.13 (m, 4H), 1.75–2.00 (m, 16H), 1.2–1.5 (m, 100H), 0.88 ppm (m, 24H); ^{13}C NMR (50 MHz, $CDCl_3$): δ = 158.4, 150.4, 149.5, 148.7, 142.9, 139.3, 138.4, 125.5, 124.7, 123.1, 116.8, 115.3, 124.7, 123.1, 116.8, 115.3, 112.8, 101.2, 70.9, 69.9, 69.7, 68.9, 40.6, 39.0, 31.8, 30.3, 29.4, 29.3, 26.2, 26.1, 26.0, 22.6, 14.0 ppm; IR (KBr): $\tilde{\nu}$ = 3352, 3051, 2954, 2923, 2870, 2852, 1627, 1577, 1212, 799 cm^{-1}; HRMS (FAB+): *m*/*z*: calcd for $C_{106}H_{179}N_4O_{10}S_2$: 1732.3062 $[M+H]^+$; found: 1732.3068; elemental analysis (%) calcd for: C 73.48, H 10.35, N 3.23, S 3.70; found: C 73.10, H 10.41, N 3.46, S 3.21.

X-ray crystal structure determination: Diffracted intensities were measured over a full sphere of the reciprocal space on an Xcalibur CCD (Oxford Diffraction) diffractometer with use of monochromated $Mo_{K\alpha}$ radiation (λ = 0.71073 Å). CrysAlisCCD and CrysAlisRed software packages[43] were used for data acquisition, extraction, and reduction. The structure was solved by direct methods as provided by SHELXS-97[44] and subsequent Fourier analyses. Refinement of atomic positions and anisotropic displacement parameters for all non-hydrogen atoms were carried out by full-matrix, least-squares methods based on F^2 (program SHELXL-97[45]). Hydrogen atoms attached to carbon were placed in geometrically idealized positions and constrained to ride on their parent atoms. They were each given an isotropic displacement parameter equal to 1.2 times the U_{eq} of their C parent.

Crystal data for 2: $C_{74}H_{114}O_6S_2$, M = 1163.77, triclinic, $P\bar{1}$, a = 7.9650(6), b = 9.549(1), c = 23.781(2) Å, α = 82.94(1)°, β = 80.60(1), γ = 79.70 (1)°, V = 1747.5(3) Å^3, T = 173 K, Z = 1, ρ_{calcd} = 1.106 g cm^{-3}, orange parallelepiped, 0.13 × 0.26 × 0.46 mm, μ = 0.125 mm^{-1}, 22714 reflections measured (θ_{max} = 25°), 6150 unique. Final R_1 = 0.0552 and wR_2 = 0.1211 for 370 refined parameters using 4156 observed reflections with $I > 2\sigma(I)$. Goodness of fit = 0.982, electron density residuals = 0.327/−0.212 e Å^{-3}.

CCDC 661776 contains the supplementary crystallographic data for this paper. These data can be obtained free of charge from The Cambridge Crystallographic Data Centre via www.ccdc.cam.ac.uk/data_request/cif.

Acknowledgements

We are grateful to the CNRS, "La Région Languedoc Roussillon" and the "AC Nanofilum" program for financial support.

[1] For a recent review on supramolecular organization of π-conjugated oligomers see F. J. M. Hoeben, P. Jonkheijm, E. W. Meijer, A. P. H. J. Schenning, *Chem. Rev.* **2005**, *105*, 1491–1546.

[2] A. L. Briseno, S. C. B. Mannsfeld, X. Lu, Y. Xiong, S. A. Jenekhe, Z. Bao, Y. Xia, *Nano Lett.* **2007**, *7*, 668–675.
[3] H. Liu, J. Komeoka, D. A. Czaplewski, H. G. Craighead, *Nano lett.* **2004**, *4*, 671–675.
[4] A. L. Briseno, S. C. B. Mannsfeld, C. Reese, J. M. Hancock, Y. Xiong, S. A. Jenekhe, Z. Bao, Y. Xia, *Nano Lett.* **2007**, *7*, 2847–2853.
[5] J. M. Moran-Mirabal, J. D. Slinker, J. A. DeFranco, S. S. Verbridge, R. Ilic, S. Flores-Torres, H. Abruna, G. G. Malliaras, H. G. Craighead, *Nano Lett.* **2007**, *7*, 458–463.
[6] S. Berson, R. De Bettignies, S. Bailly, S. Guillerez, *Adv. Funct. Mater.* **2007**, *17*, 1377–1384.
[7] R. Wang, C. Geiger, L. Chen, B. Swanson, D. G. Whitten, *J. Am. Chem. Soc.* **2000**, *122*, 2399–2400.
[8] A. Ajayaghosh, S. J. George, *J. Am. Chem. Soc.* **2001**, *123*, 5148–5149.
[9] a) J. van Esch, R. M. Kellog, B. L. Feringa, *Tetrahedron Lett.* **1997**, *38*, 281–284; b) J. van Esch, S. De Feyter, R. M. Kellog, F. De Schryver, B. L. Feringa, *Chem. Eur. J.* **1997**, *3*, 1238–1243; c) F. S. Schoonbeek, J. van Esch, B. Wegewijs, D. B. A. Rep, M. P. de Haas, T. M. Klapwijk, R. M. Kellog, B. L. Feringa, *Angew. Chem.* **1999**, *111*, 1486–1490; *Angew. Chem. Int. Ed.* **1999**, *38*, 1393–1397.
[10] D. B. A. Rep, R. Roelfsema, J. H. van Esch, F. S. Schoonbeek, R. M. Kellog, B. L. Feringa, T. T. M. Palstra, T. M. Klapwijk, *Adv. Mater.* **2000**, *12*, 563–566.
[11] A. Gesquière, S. De Feyter, F. C. De Schryver, F. S. Schoonbeek, J. H. van Esch, R. M. Kellog, B. L. Feringa, *Nano Lett.* **2001**, *1*, 201–206.
[12] A. P. H. J. Schenning, E. W. Meijer, *J. Chem. Soc. Chem. Commun.* **2005**, 3245–3258.
[13] S. Lois, J.-C. Florès, J.-P. Lère-Porte, F. Serein-Spirau, J. J. E. Moreau, K. Miqueu, J.-M. Sotiropoulos, P. Baylère, M. Tillard, C. Belin, *Eur. J. Org. Chem.*, **2007**, *24*, 4019–4031.
[14] T. Kobayashi, T. Seki, K. Ichimura, *J. Chem. Soc. Chem. Commun.* **2000**, 1193–1194.
[15] J. M. Warman, G. H. Gellinck, M. P. de Haas, *J. Phys. Condens. Matter* **2002**, *14*, 9935–9954.
[16] P. H. Aubert, M. Knipper, L. Groenendaals, L. Lutsen, J. Manca, D. Vanderzande, *Macromolecules* **2004**, *37*, 4087–4098.
[17] C. A. Bartram, D. A. Battye, C. R. Worthing, *J. Chem. Soc. Abstr.* **1963**, 4691–4693.
[18] K. Kaifu, A. Nishiki, T. Koyano, January 07, **1998**, EP0816914.
[19] A. S. Castanet, F. Colobert, P.-E. Broutin, *Tetrahedron Lett.* **2002**, *43*, 5047–5048.
[20] a) M. George, S. L. Snyder, P. Terech, C. J. Glinka, R. G. Weiss, *J. Am. Chem. Soc.* **2003**, *125*, 10278–10283; b) S. Wellinghoff, J. Shaw, E. Baer, *Macromolecules* **1979**, *12*, 932–939.
[21] a) M. de Loos, J. van Esch, I. Stokroos, R. M. Kellogg, B. L. Feringa, *J. Am. Chem. Soc.* **1997**, *119*, 12675–12676; b) H. M. Tan, A. Moet, A. Hiltner, E. Baer, *Macromolecules* **1983**, *16*, 28–34; c) A. Takahashi, M. Sakai, T. Kato, *Polym. J.* **1980**, *12*, 335–341.
[22] P. Terech, R. G. Weiss, *Chem. Rev.* **1997**, *97*, 3133–3160.
[23] O. J. Dautel, M. Robitzer, J.-P. Lère-Porte, F. Serein-Spirau, J. J. E. Moreau, *J. Am. Chem. Soc.*, **2006**, *128*, 16213–16223.
[24] J. Jadzyn, M. Stockhauser, B. Zywucki, *J. Phys. Chem.* **1987**, *91*, 754–757.
[25] L. G. S. Brooker, F. L. White, D. W. Heseltine, G. H. Keyes, S. G. Dent, E. J. VanLare, *J. Photogr. Sci.* **1953**, *1*, 173.
[26] a) E. E. Jelly, *Nature* **1936**, *138*, 1009; b) G. Scheibe, *Angew. Chem.* **1936**, *48*, 563.
[27] M. Kasha, H. R. Rawls, M. A. El-Bayoumi, *Pure Appl. Chem.* **1965**, *11*, 371–392.
[28] A. Schenning, P. Jonkheijm, E. Peeters, W. Meijer, *J. Am. Chem. Soc.* **2001**, *123*, 409–416.
[29] D. G. Whitten, *Acc. Chem. Res.* **1993**, *26*, 502–509.
[30] M. D. Curtis, J. Cao, J. W. Kampf, *J. Am. Chem. Soc.* **2004**, *126*, 4318–4328.
[31] X. Zhao, Y. L. Chang, F. W. Fowler, J. W. Lauher, *J. Am. Chem. Soc.* **1990**, *112*, 6627–6634.
[32] T. Heim, K. Lmimouni, D. Vuillaume, *Nano Lett.* **2004**, *4*, 2145–2150.
[33] T. Heim, T. Melin, D. Deresmes, D. Vuillaume, *Appl. Phys. Lett.* **2004**, *85* (3), 2637–2639.
[34] I. Horcas, R. Fernández, J. M. Gómez-Rodríguez, J. Colchero, J. Gómez-Herrero, A. M. Baro, *Rev. Sci. Instrum.* **2007**, *78*, 013705.
[35] T. Melin, H. Diesinger, D. Deresmes, D. Stievenard, *Phys. Rev. B* **2004**, *69*, 035321.
[36] In the present case, g is given by $1+(2t_{ox}\varepsilon_R/h\varepsilon_{ox})$ with t_{ox} the oxide thickness (4 nm), h the nanorod height ($\approx$2.5 nm), and ε_{ox} and ε_ρ the oxide and nanorod dielectric constants (3.9 and $\approx$3, respectively).
[37] The lateral resolution is inversely proportional to the tip–substrate distance. Its value can be deduced by comparison of a topographic profile and the EFM profile of charged silicon small nanoparticles with use of similar equipment and measurement conditions; see T. Mélin, H. Diesinger, D. Deresmes, D. Stiévenard, *Phys. Rev. Lett.* **2004**, *92*, 166101.
[38] This increase in size cannot be explained by the larger V_{inj} in this latter case (-3 V instead of -2 V). In such a 4 nm-thick oxide, the corresponding size increase is limited to a few tens of nm for a 1 V increase of V_{inj}. T. Melin, private communication.
[39] For these nanorings, with an average height $h \approx 10$ nm, $g \approx 1.6$ is used in Eq. (1).
[40] M. Mayor, C. Didschies, *Angew. Chem.* **2003**, *115*, 3284–3287; *Angew. Chem. Int. Ed.* **2003**, *42*, 3176–3179.
[41] D. M. Johansson, X. Wang, T. Johansson, O. Inganaes, G. Yu, G. Srdanov, M. R. Andersson, *Macromolecules* **2002**, *35*, 4997–5003.
[42] M. Bouachrine, J. -P. Lère-Porte, J. J. E. Moreau, F. Serein-Spirau, C. Torreilles, *J. Mater. Chem.* **2000**, *10*, 263–268.
[43] *CrysAlisCCD and CrysAlisRed 169 software package*, Oxford Diffraction, Ltd. Abingdon (UK), **2001**.
[44] G. M. Sheldrick, *SHELXS-97*: *A Program for Crystal Structures Solution*, University of Göttingen (Germany), **1997**.
[45] G. M. Sheldrick, *SHELXL-97*: *A Program for Refining Crystal Structures*, University of Göttingen (Germany), **1997**.

Received: October 16, 2007
Published online: March 25, 2008

